

# Direct Visualization of Symmetry Breaking During Janus Nanoparticle Formation

Gabriel Loget, Tung C. Lee, Richard W. Taylor, Sumeet Mahajan, Olivia Nicoletti, Samuel T. Jones, Richard J. Coulston, Véronique Lapeyre, Patrick Garrigue, Paul A. Midgley, Oren A. Scherman, Jeremy J. Baumberg, and Alexander Kuhn\*

*The straight-forward synthesis of Janus nanoparticles composed of Ag and AgBr is reported. For their formation, cucurbit[n]uril (CB)-stabilized AgBr nanoparticles are first generated in water by precipitation. Subsequent irradiation with an electron beam transforms a fraction of each AgBr nanoparticle into Ag<sup>0</sup>, leading to well-defined Janus particles, stabilized by the binding of CB to the surface of both AgBr and Ag<sup>0</sup>. With the silver ion reduction being triggered by the electron beam, the progress of the transformation can be directly monitored with a transmission electron microscope.*

## 1. Introduction

Nanoparticles (NPs) with an asymmetry in polarity or chemical composition, so-called Janus particles (JPs)<sup>[1–3]</sup> referring to the double-faced Roman god, or asymmetric patchy particles,<sup>[4,5]</sup> are of great interest, since they show a strong potential for various applications ranging from therapeutics<sup>[6]</sup> to catalysis.<sup>[7]</sup> In particular metal-semiconductor (M-SC) nanojunctions are attracting a lot of attention, because they lead

to very efficient photocatalysts.<sup>[8,9]</sup> Several methods have been reported to generate M-SC JPs such as metal deposition on one tip of CdS nanorods<sup>[10,11]</sup> or CdSe-seeded CdS nanorods,<sup>[12,13]</sup> PbSe growth from a single facet of Au-Fe<sub>3</sub>O<sub>4</sub> NPs<sup>[14]</sup> and annealing of FePt-CdS<sup>[15]</sup> or  $\gamma$ -Fe<sub>2</sub>O<sub>3</sub>-CdSe<sup>[16]</sup> core-shell particles. In this context silver/silver halide (Ag/AgX) NPs have recently been reported to be very efficient plasmonic photocatalysts.<sup>[17,18]</sup> Moreover, on account of the antimicrobial properties of Ag and AgX NPs,<sup>[19]</sup> a combination of both in the form of Ag/AgX JPs is also very promising for therapeutics, as they can be generated for example as dimer nanocrystals.<sup>[20]</sup> However, reliable single step syntheses of JPs remain to be established, particularly those that are amenable to scale-up.

Cucurbit[n]urils (CB[n]s) are pumpkin-shaped symmetric macrocycles composed of glycoluril sub-units (**Figure 1a**). The molecular construct of CB[n]s consists of a highly symmetric hydrophobic cavity with two polar carbonyl portals. CB[n]s can act as supramolecular hosts that selectively form inclusion complexes with a wide variety of small organic guest molecules.<sup>[21]</sup> Recently, native CB[n]s were shown to have significant binding interactions with the surfaces of noble metals.<sup>[22,23]</sup> Meanwhile, CB[n]s have been utilized as stabilizing ligands for noble metal nanoparticles (NPs), such as that of gold,<sup>[24–27]</sup> silver,<sup>[28,29]</sup> and palladium.<sup>[30]</sup> These macrocycles have attracted much interest, since their properties and importance in various chemical domains are increasingly highlighted.

Direct visualization of chemical events at the nanoscale such as the growth of carbon nanofibers<sup>[31]</sup> or graphene<sup>[32]</sup> formation and isomerization<sup>[33]</sup> has been reported previously, however

G. Loget, V. Lapeyre, P. Garrigue, Prof. A. Kuhn  
ISM, UMR 5255

Université de Bordeaux  
33607 Pessac, France  
E-mail: kuhn@enscbp.fr

Dr. T.-C. Lee, S. T. Jones, Dr. R. J. Coulston,  
Dr. O. A. Scherman  
Melville Laboratory for Polymer Synthesis  
Department of Chemistry  
University of Cambridge  
Cambridge, CB2 1EW, UK

R. W. Taylor, Dr. S. Mahajan, Prof. J. J. Baumberg  
NanoPhotonics Centre  
Cavendish Laboratory  
University of Cambridge  
Cambridge CB3 0HE, UK

O. Nicoletti, Prof. P. A. Midgley  
Department of Materials Science and Metallurgy  
University of Cambridge  
Pembroke Street, CB2 3QZ, Cambridge, UK

DOI: 10.1002/sml.201200546



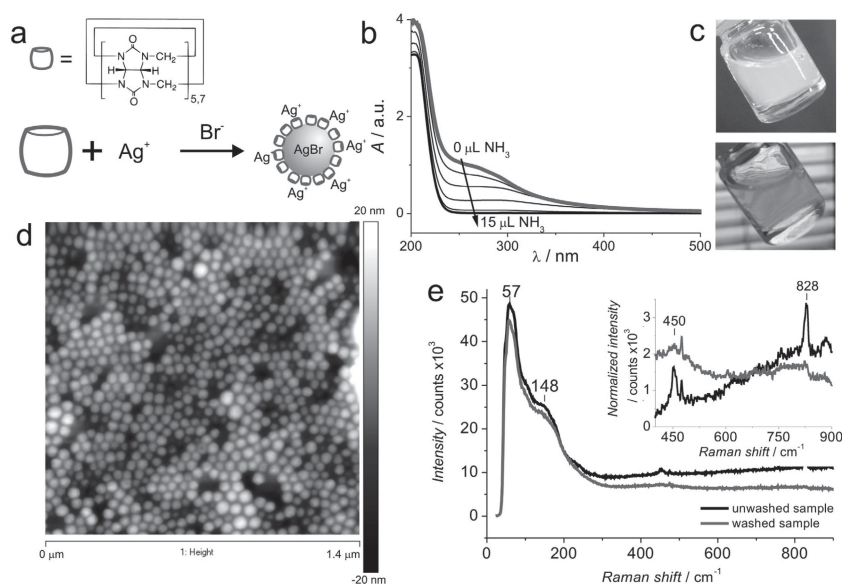


**Figure 1.** Characterization of CB[5] capped AgBr NPs. a) Scheme of AgBr NP precipitation in the presence of CB[5,7]. b) UV-visible absorption spectrum of AgBr NPs (bold spectrum) and during sequential particle dissolution with ammonia. c) Reflection (top) and transmission (bottom) images of a CB[5]-capped AgBr suspension. d) AFM height image of the CB[5]-capped AgBr nanoparticles. e) Raman spectra of unwashed (black) and washed (gray) CB[5]-capped AgBr suspensions. Inset: enlargement of the normalized CB[5] Raman signal.

direct visualization of Janus nanoparticle formation has never been demonstrated. Mulvaney and coworkers reported TEM evidence for a spontaneous symmetry breaking in the case of silver-silica core-shell particles induced through the generation of AgI by  $I_2$ .<sup>[34]</sup> In their work, however, JP formation is not induced by exposure to an electron beam and therefore cannot be monitored in real-time by the electron microscope.

In this communication, we report for the first time the aqueous phase synthesis of CB-stabilized AgBr nanoparticles with a narrow size distribution. The binding interactions between CBs and the surface of both, AgBr and  $Ag^0$  favor the formation of  $Ag^0$  nanoparticles from AgBr under electron beam irradiation. This in turn enables the direct visualization with a transmission electron microscope of the electron-beam induced partial reduction of CB[n]-stabilized AgBr NPs into  $Ag^0$  in an asymmetric manner, leading to JPs with controllable morphologies. These observations, concerning the *in situ* symmetry-breaking, allow new insights relevant for the elaboration of new concepts for synthesizing JPs.

## 2. Results and Discussion

Precipitation from aqueous solution of  $AgNO_3$  and CB[5] takes place over 24 h in the dark with the  $n_{AgNO_3}/n_{CB[5]}$  molar ratio equal to one, and leads to stable suspensions exhibiting white reflection and orange transmission (Figure 1c).

The white color is typical for silver-halide NP suspensions and is attributed to the presence of a small amount of bromide ions present in the synthesized CB[5]. The CB[5] purification process, which involves a bromide containing ionic liquid, introduces the trace bromide ions.<sup>[37]</sup> The total bromine amount in CB[5] was determined by ICP-MS

analysis to be  $3.01 \times 10^{-4}$ %wt. A typical UV-visible spectrum of this suspension ( $C_{CB[5]} = C_{AgNO_3} = 0.34 \times 10^{-4}$  M) can be seen in Figure 1b. The strong peak around 200 nm corresponds to  $AgNO_3$  absorption, while the shoulder-like absorption in the visible region is attributed to that of silver halide NPs, as previously reported for AgBr NPs by Ray et al.<sup>[36]</sup> The assignment of these peaks to silver-halide NPs was further confirmed by a decrease of the absorption upon addition of ammonia to the quartz cuvette, which leads to the dissolution of the silver halide (Figure 1b). No characteristic  $Ag^0$  NP plasmon peak (around 400 nm) is observed before or after the dissolution by ammonia, which suggests the absence of  $Ag^0$  NPs in solution. AFM measurements revealed the shape of the AgBr NPs to be spherical with a diameter of  $47 \pm 3$  nm, that has been determined by measuring their horizontal size (Figure 1d).

The bromide content in solution was governed by the CB[5] batch employed, but even when using different CB[5]

batches, similar NPs were obtained in every case. It is worth noting that addition of sodium bromide to the solution (from 5 to 50 mM) did not affect the shape and size of the NPs. Using a specific purified CB[7] batch, that did not contain any  $Br^-$ , no NPs were obtained. However, addition of potassium bromide in as low a concentration as  $1.2 \times 10^{-5}$  M induced the formation of CB[7]-capped AgBr NPs.

In order to investigate the NP composition in more detail, liquid phase Raman spectroscopy was also performed with the initial and the centrifuged suspensions (Figure 1e). In both samples, the presence of a silver-halide is observed with a characteristic Raman fingerprint below  $300\text{ cm}^{-1}$ ,<sup>[38]</sup> and the presence of CB[5] is confirmed by its characteristic Raman peaks at  $450$  and  $828\text{ cm}^{-1}$  in both spectra.<sup>[23]</sup> The centrifugation/washing process, which allows the isolation of AgBr NPs by removal of soluble compounds, results in a significant decrease in the intensity of the CB[5] peaks in the Raman spectrum compared to the unwashed sample. This means that CB[5] is not a component of the bulk NPs, but rather acts as a stabilizing ligand on the surface of AgBr NPs. A further confirmation of this is the fact that without CB[n] in solution, AgBr precipitation leads to the formation of large particles, that settle at the bottom of the vial (see below).

This control experiment indicates that CB[5] promotes the formation of monodisperse and stable AgBr NPs through  $Ag^+$  binding to the portal carbonyls by electrostatic interactions (see Figure 1a), because it is well documented that CB[n] macrocycles have a strong affinity to cations.<sup>[39]</sup> This is consistent with Zeta potential measurements of the colloidal suspensions, which revealed a surface potential of +43 mV for the NPs. The hydrodynamic diameter of the colloidal particles, determined by DLS, was found to be  $90.6 \pm 0.2$  nm. This is twice as much as the value observed by AFM, which can

be partly due to solvent effects, but also to aggregates containing three to four nanoparticles based on the NP diameters obtained from AFM data. The colloidal diameter value does not vary significantly when the sample is diluted by a factor of up to 20, meaning that the observed aggregates are not a result of the non-specific aggregation of charged colloids, which typically is concentration-dependent. The result suggests that the aggregates are bridged by CB[5], similar to what has been shown for CB-gold NP aggregates in previous publications,<sup>[24,25]</sup> confirming the capping role of CB[5]. CB[*n*]s are already known to have an affinity for certain metals,<sup>[22,23]</sup> and the synthesis of CB[*n*]-capped metal nanoparticles has been previously reported.<sup>[24–30]</sup> Here we present the first example of CB[*n*]-stabilized metal halide NPs, which may be extended in the near future to a larger family of nanoparticles, based on other metals and/or halides.

The obtained NPs exhibit a high reactivity when visualized in the TEM. Indeed, when exposed to the electron beam, they demonstrate a clear asymmetric evolution of their composition

and morphology, which resulted in JPs composed of a black and a grey part (**Figure 2b**). Scanning transmission electron microscopy-energy dispersive X-ray spectroscopy (STEM-EDX) analysis, carried out on an untypically big object (owing to the higher stability of the particle under the electron-beam), revealed the black part to be silver and the grey part to be AgBr (Figure 2d). We attributed this evolution to the direct reduction of the AgBr component by the electron beam as shown in Figure 2a. The generation of a black seed occurs very quickly, so that it was impossible to record a TEM micrograph of the AgBr NP without any Ag<sup>0</sup>. It has been therefore necessary to employ AFM to image the initial AgBr NPs and then follow the subsequent seed growth in real time under the e-beam, which is used simultaneously for imaging and to deliver the electrons for Ag<sup>+</sup> reduction (Figure 2b). It is important to note that the phenomenon was more pronounced in parts of the samples where the beam was focused, but was also effective on a much larger area of the TEM grids. For instance, imaging a grid area at magnification of 49,000× induced the generation of black silver seeds over at least a 100 μm × 100 μm square of the grid mesh.

Similar results were observed using two different TEM instruments (FEI Tecnai 12 and Technai G2), confirming clearly that the phenomenon is related to an inherent property of the NP material. Analyzing the growth process in more details (shown in Figure 2c), one can clearly note that the grey AgBr is the “feeder” part for the Ag<sup>0</sup> seed, which grows while the AgBr decreases in size until its complete consumption (55 minutes for the NPs with a typical size around 30 nm). Therefore, the Ag<sup>0</sup> component can grow by more than 5 nm in size, while the AgBr is being consumed (Figure 2c).

In order to investigate the mechanism, we also studied nanoparticles of AgCl and AgBr synthesized without any CB[*n*]. Although the AgCl NPs showed an observable reactivity on account of TEM-induced reduction, no symmetry breaking could be observed. On the other hand, an asymmetric growth of a silver component was observed for the unstabilized AgBr NPs, leading to asymmetric particles, but with a much less well-defined morphology (**Figure 3d**). Due to the absence of the CB[*n*] stabilizing agent during the AgBr precipitation, most of the material settled at the bottom of the vial (Figure 3d, inset), and only a few AgBr NPs with ill-defined shape were observed. The size distribution was estimated by measuring the length of the particles from one extremity of the metal bulb to the opposite extremity of the AgBr component. As shown in Figure 3e, the particles obtained without CB[*n*] are significantly larger compared to those

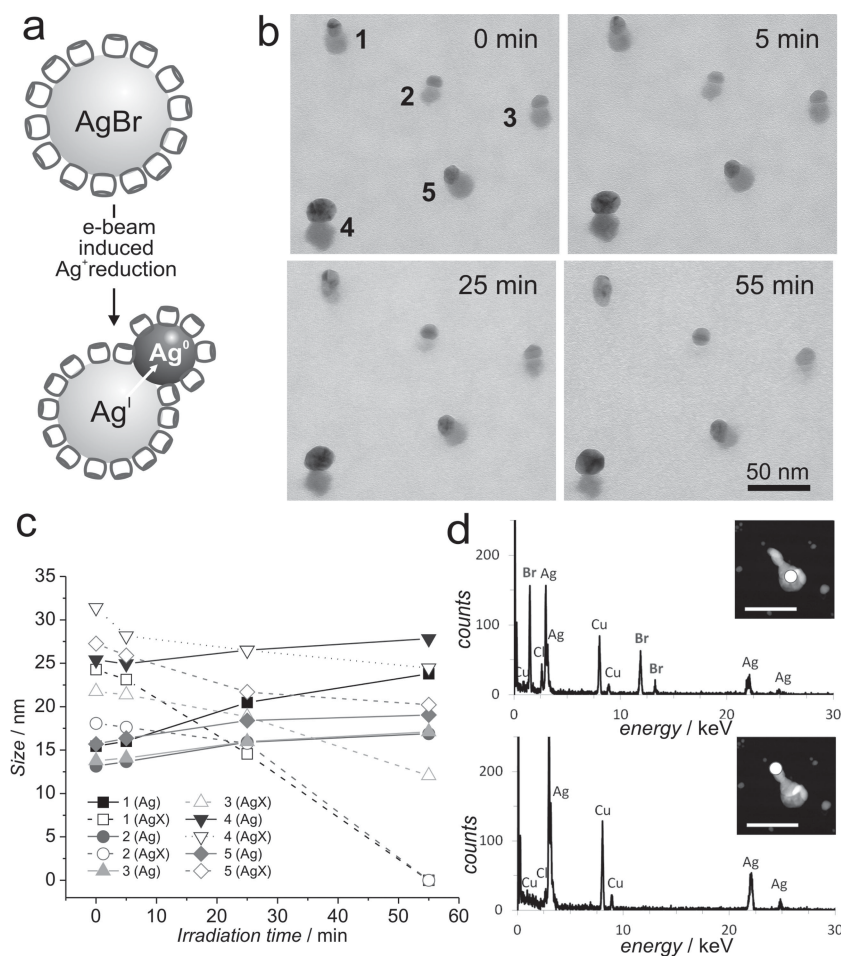


**Figure 2.** Direct visualization of the symmetry breaking of Ag<sup>0</sup>-AgBr NPs. a) Scheme of the mechanism. b) TEM pictures showing the morphological evolution of CB[5]-capped Ag<sup>0</sup>-AgBr particles as a function of time. c) Kinetics data showing the size evolution of the Ag<sup>0</sup> and AgBr parts for each particle numbered in Figure 2b. d) STEM-EDX analysis of the different parts of a Ag<sup>0</sup>-AgBr NP. Top, STEM-EDX analysis of the AgBr feeder part. Bottom, STEM-EDX analysis of the Ag<sup>0</sup> bulb part. Insets: HAADF images of the analyzed NP, the white spot shows the location of the EDX analysis, scale bars: 200 nm. The Cu signal originates from the Cu grid support.

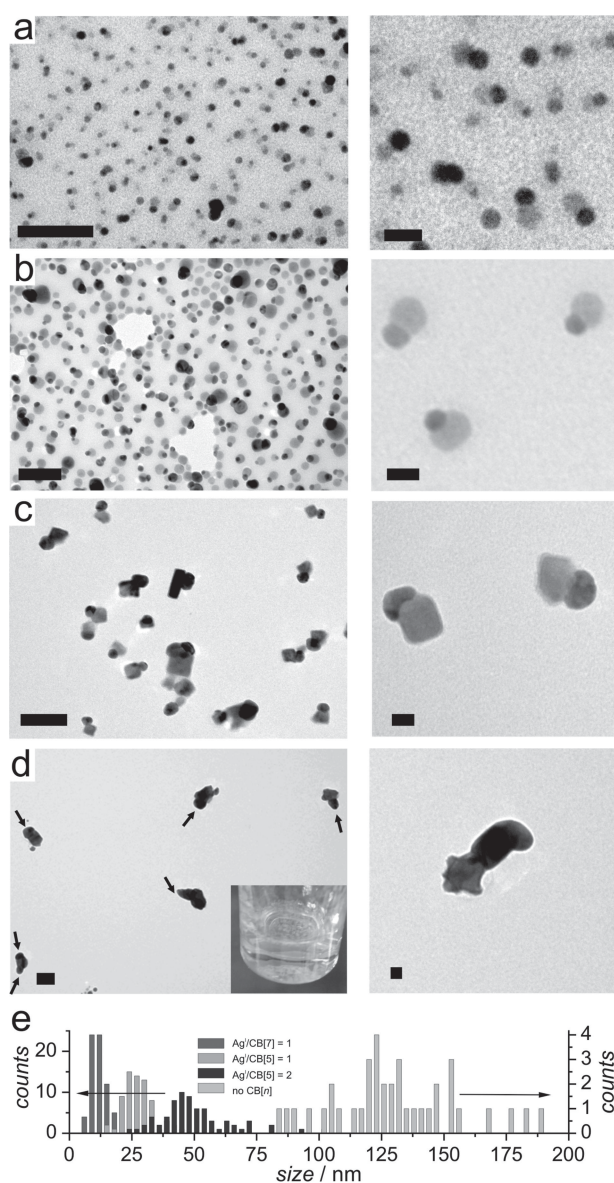


**Figure 3.** TEM pictures of  $\text{Ag}^0$ -AgBr Janus particles. a) Particles obtained using  $\text{Ag}^0/\text{CB}[7] = 1$  (scale bar left: 100 nm, right: 20 nm). b) Particles obtained using  $\text{Ag}^0/\text{CB}[5] = 1$  (scale bar left: 100 nm, right: 20 nm). c) Particles obtained using  $\text{Ag}^0/\text{CB}[5] = 2$  (scale bar left: 100 nm, right: 20 nm). d) Particles obtained without  $\text{CB}[n]$  (scale bar left: 100 nm, right: 20 nm). e) Size distributions of the JPs obtained with the different mixtures.

that are  $\text{CB}[n]$ -capped. The silver growth observed on these larger particles is also very different since the AgBr component appears to be darker than the AgBr of the  $\text{CB}[5]$ -capped NPs, suggesting the formation of a  $\text{Ag}^0$  layer all around the AgBr. The silver components, grown under the influence of the electron beam, can still be identified and are indicated by arrows in Figure 3d. While the silver, grown on the  $\text{CB}[5]$ -capped AgBr NPs, is spherical in nature, the silver growth on the uncapped NPs appears much less well-defined, and in some cases even multiple bulbs can grow on a single AgBr particle (Figure 3d, left bottom). We conclude that the asymmetric  $\text{Ag}^0$  growth is a phenomenon related to the presence of AgBr, which is strongly enhanced by the presence of  $\text{CB}[5]$

on the AgBr NPs surfaces. Beyond promoting the monodispersity of the AgBr NPs, the  $\text{CB}[5]$  layer protects the AgBr part from a complete, TEM-induced reduction. The  $\text{Ag}^0$  components are located at very different positions on the initial AgBr particle with respect to the surface of the TEM grid (Figure 2a,3), which indicates that the symmetry breaking is not a consequence of the surface immobilization of the NPs.

It was found that the  $n_{\text{AgNO}_3}/n_{\text{CB}[n]}$  molar ratio strongly influences the AgBr NP morphology and shape, which in turn has an impact on the final appearance of the resulting JPs. We illustrate this structural versatility in Figure 3. As already discussed above, when the  $n_{\text{AgNO}_3}/n_{\text{CB}[5]}$  molar ratio is 1, the AgBr NPs are spherical. Figure 3b shows a picture of well separated AgBr- $\text{Ag}^0$  NPs and the conversion yield into JPs is more than 75%. The average JP size was found to be around 25 nm (Figure 3e). Using a smaller relative  $\text{CB}[5]$  concentration in solution favours the formation of larger NPs, since fewer CBs are available for surface stabilisation, as shown for the case of  $n_{\text{AgNO}_3}/n_{\text{CB}[5]} = 2$  in Figure 3c. Interestingly, most of these NPs prepared from ratios greater than one exhibit cubic or rectangular morphologies, and a majority of the resulting JPs are about 45 nm across. The  $\text{Ag}^0$  patch grows in some cases at an AgBr NP face and in other cases at a NP edge. This suggests that the nucleation mechanism of the reduction does not necessarily happen at energetically favoured sites. Probably due to its larger outer diameter compared to  $\text{CB}[5]$ ,<sup>[40]</sup> the use of  $\text{CB}[7]$  with a molar ratio of 1 leads to smaller AgBr NPs, as shown in Figure 3a and 3e. When  $\text{CB}[7]$  is used, JPs of about 10 nm size are observed with a very good synthetic yield. Notably, in all cases where CB is present as a capping agent, the  $\text{Ag}^0$  bulbs have a similar spherical morphology.

### 3. Conclusion

In this report, we present for the first time the straight forward aqueous-phase synthesis of  $\text{CB}[n]$ -stabilized AgBr NPs with a narrow size distribution.  $\text{CB}[n]$ s, acting as stabilizing agents, promote the formation of monodisperse AgBr nanoparticle suspensions, which are stable for over a month. The  $\text{AgNO}_3/\text{CB}[n]$  molar ratios and the  $\text{CB}[n]$  type were found to be key parameters for controlling the NP morphologies and sizes. Most importantly, we showed that the asymmetric reduction of these NPs, leading to growth of  $\text{Ag}^0$  patches can be achieved and directly observed under the influence of electron irradiation. Depending on the AgBr particle shape, the generated JP morphology can be tuned. Apart from the mere academic curiosity to understand how CBs can control the crucial asymmetric reduction process, we expect this phenomenon to be useful for practical applications ranging from photocatalysis<sup>[17,18]</sup> to therapeutics.<sup>[19]</sup> JP synthesis is an important and fast evolving research area, and therefore these findings will be of interest for the development of new synthetic methods for such bifunctional objects. Firstly, this reported reduction mechanism may be used for generating other metal JPs, and secondly, the  $\text{Ag}^0$ -AgBr particles themselves can serve as synthetic platforms for the generation of a wide range of new JPs due to their chemical anisotropy.<sup>[41,42]</sup> Therefore this approach constitutes an interesting enrichment of the large variety of

synthetic methods reported in the literature.<sup>[43]</sup> Research is now under way to completely elucidate the mechanism of the symmetry breaking and to investigate the bulk reduction of CB stabilized AgBr NPs by chemical or photochemical means.

## 4. Experimental Section

**Solutions and Chemicals:** Silver nitrate (>99%, titration grade, Sigma Aldrich), ammonia (25%, ISO reagent, Riedel-de Haën), sodium bromide (>99%, ACS reagent, Sigma Aldrich), and hydrochloric acid (1 M ProLabo) were used as received. CB[7] and CB[5] were synthesized,<sup>[35]</sup> separated and purified<sup>[37]</sup> according to already published procedures. The bromide-free CB[7] was purified according to reported procedures by Kim et al.<sup>[35]</sup> Solutions were prepared using milliQ water (resistivity = 18 MΩ cm) in glass vials.

**Preparation of AgBr and AgCl Particles:** AgBr and AgCl were respectively prepared by precipitating 0.5 mL of an 11.7 mM AgNO<sub>3</sub> aqueous solution with 0.36 mL of 24 mM HCl, and 0.16 mL of a 6 mM AgNO<sub>3</sub> aqueous solution with 0.12 mL of 6 mM NaBr during ~24 h in the dark. Though a part of the precipitate settled at the bottom of the vials, the supernatant contained a sufficient amount of NPs that was transferred and observed on the TEM grids.

**Preparation of CB[n]-Capped AgBr Nanoparticles:** The typical procedure for preparing CB[5]-capped AgBr NPs using a ratio of  $n_{\text{AgNO}_3}/n_{\text{CB}[5]} = 1$  consisted in mixing 0.36 mL of a 16 mM aqueous CB[5] solution and 0.48 mL of a 12 mM aqueous AgNO<sub>3</sub> solution in a vial. A typical procedure for preparing CB[7]-capped AgBr NPs consisted in mixing 0.36 mL of a 8 mM aqueous CB[7] solution and 0.48 mL of a 6 mM aqueous AgNO<sub>3</sub> solution in a vial. The vials were then placed in the dark for ~24 h. White solutions with orange reflectivity were obtained. Decreasing the CB[5]-AgNO<sub>3</sub> concentrations by a factor of 4 was found to lead to the same results.

**DLS and Zeta Potential Measurement:** Dynamic light scattering (DLS) and Zeta potential measurements were carried out with a Zeta-sizer nano-ZS (Malvern) at 25 °C. Five measurements were carried out for each sample to ensure good reproducibility.

**UV-visible and Raman Spectroscopy:** UV spectra were recorded with suspensions diluted ten times with mQ water in 2 mL quartz cells with a Varian Cary 100 scan UV-visible spectrophotometer. Raman spectra were collected with a 532 nm laser on an InVia Renishaw system under 2 mW incident power. Each spectrum was acquired with 3 exposures of 10 s each. An edge filter (cut-off ~50 cm<sup>-1</sup>) to block Rayleigh scattering and a 2400 lines/mm grating was used, which gave a resolution of approximately 2 cm<sup>-1</sup>.

**AFM Imaging:** Atomic force microscopy (AFM) imaging (Veeco multimode 8) was carried out in the Scan-assist mode on cleaved highly oriented pyrolytic graphite (HOPG) substrates modified by evaporating a drop of particle suspension on it.

**TEM Imaging:** In order to test the reproducibility, two sample preparation procedures and two transmission electron microscopes (TEM) were used. For the first protocol, TEM grids (Agar Scientific, Formvar/carbon 200 mesh Cu) were prepared by placing a droplet on the grid and sucking it through the grid from below. This procedure was repeated three times with the particle suspension and then three times with mQ water in order to wash the sample. A FEI Tecnai 12 equipped with an Orius SC1000 11MPx (GATAN) camera was used to visualize the particles.

The second procedure consisted in placing one drop of sample solution onto a glow-discharged carbon coated TEM grid

(300 mesh, Cu) for ~60 s. Excess sample was removed carefully with a filter paper. The sample loaded grid was washed twice with deionized water to remove salts and dried in air. TEM images were captured under an acceleration voltage of 120 kV using a FEI Tecnai G2 TEM.

Time-resolved morphological evolution of CB[5]-capped Ag<sup>0</sup>-AgBr particles was studied by focusing an electron beam onto a selected area of interest. Drifting of the beam and/or sample was manually corrected during the experiment. Sizes distribution measurements were carried out by measuring the longest axis of JPs. For data of the growth kinetics, the average of the major and the minor axis measurements for each JP part is reported.

**STEM-EDX Experiments:** Scanning transmission electron microscopy–energy dispersive X-ray spectroscopy (STEM-EDX) was performed on samples prepared as in the previous section. The measurements were conducted on a FEI Tecnai F20 FEGTEM operated at 200 kV equipped with a cold field-emission gun and an EDAX r-TEM ultra-thin window (UTW) X-ray detector. The electron probe size was set to around 2 nm and the acquisition time was set to 60 s per EDX spectrum. High angle annular dark field (HAADF) images were collected to determine the region of interest for EDX analysis. The EDX spectra are here presented unprocessed.

## Acknowledgements

This work is funded by the CUBIHOLE Project in the frame of the European NanoSci-Era+ action under contract ANR-08-NSCI-008-01, EPSRC EP/H007024/1 and EP/G060649/1. ON and PAM acknowledge financial support from the European FP 6 program under a contract for an Integrated Infrastructure Initiative (026019 ESTEEM).

- [1] A. Perro, S. Reculosa, S. Ravaine, E. Bourgeat-Lami, E. Duguet, *J. Mater. Chem.* **2005**, *15*, 3745–3760.
- [2] A. Walther, A. H. E. Müller, *Soft Matter* **2008**, *4*, 663–668.
- [3] S. Jiang, Q. Chen, M. Tripathy, E. Luijten, K. S. Schweizer, S. Granick, *Adv. Mater.* **2010**, *22*, 1060–1071.
- [4] S. C. Glotzer, M. J. Solomon, *Nat. Mater.* **2007**, *6*, 557–562.
- [5] J. Du, R. K. O'Reilly, *Chem. Soc. Rev.* **2011**, *40*, 2402–2416.
- [6] S.-H. Hu, X. Gao, *J. Am. Chem. Soc.* **2010**, *132*, 7234–7237.
- [7] D. J. Cole-Hamilton, *Science* **2010**, *327*, 41–42.
- [8] X. Fu, J. Liu, H. Yang, J. Sun, X. Li, X. Zhang, Y. Jia, *Mater. Chem. Phys.* **2011**, *130*, 334–339.
- [9] S. Pradhan, D. Ghosh, S. Chen, *ACS App. Mater. Interfaces* **2009**, *1*, 2060–2065.
- [10] S. E. Habas, P. Yang, T. Mokari, *J. Am. Chem. Soc.* **2008**, *130*, 3294–3295.
- [11] T. Mokari, C. G. Sztrum, A. Salant, E. Rabani, U. Banin, *Nat. Mater.* **2005**, *4*, 855–863.
- [12] S. Deka, A. Falqui, G. Bertoni, C. Sangregorio, G. Poneti, G. Morello, M. D. Giorgi, C. Giannini, R. Cingolani, L. Manna, P. D. Cozzoli, *J. Am. Chem. Soc.* **2009**, *131*, 12817–12828.
- [13] S. Chakraborty, J. A. Yang, Y. M. Tan, N. Mishra, Y. Chan, *Angew. Chem. Int. Ed.* **2010**, *49*, 2888–2892.
- [14] W. Shi, Y. Sahoo, H. Zeng, Y. Ding, M. T. Swihart, P. N. Prasad, *Adv. Mater.* **2006**, *18*, 1889–1894.
- [15] H. Gu, R. Zheng, X. Zhang, B. Xu, *J. Am. Chem. Soc.* **2004**, *126*, 5664–5665.

- [16] K.-W. Kwon, M. Shim, *J. Am. Chem. Soc.* **2005**, *127*, 10269–10275.
- [17] P. Wang, B. Huang, Z. Lou, X. Zhang, X. Qin, Y. Dai, Z. Zheng, X. Wang, *Chem. Eur. J.* **2010**, *16*, 538–544.
- [18] P. Wang, B. Huang, X. Zhang, X. Qin, Y. Dai, Z. Wang, Z. Lou, *ChemCatChem* **2011**, *3*, 360–364.
- [19] O. Choi, K. K. Deng, N.-J. Kim, L. Ross Jr., R. Y. Surampalli, Z. Hu, *Water Res.* **2008**, *42*, 3066–3074.
- [20] A. E. Saunders, I. Popov, U. Banin, *Z. Anorg. Allg. Chem.* **2007**, *633*, 2414–2419.
- [21] J. Lagona, P. Mukhopadhyay, S. Chakrabarti, L. Isaacs, *Angew. Chem. Int. Ed.* **2005**, *44*, 4844–4870.
- [22] Q. An, G. Li, C. Tao, Y. Li, Y. Wu, W. Zhang, *Chem. Commun.* **2008**, 1989–1991.
- [23] S. Mahajan, T.-C. Lee, F. Biedermann, J. T. Hugall, J. J. Baumberg, O. A. Scherman, *Phys. Chem. Chem. Phys.* **2010**, *12*, 10429–10433.
- [24] T.-C. Lee, O. A. Scherman, *Chem. Commun.* **2010**, *46*, 2438–2440.
- [25] T.-C. Lee, O. A. Scherman, *Chem. Eur. J.* **2012**, *18*, 1628–1633.
- [26] R. W. Taylor, T.-C. Lee, O. A. Scherman, R. Esteban, J. Aizpurua, F. M. Huang, J. J. Baumberg, S. Mahajan, *ACS Nano* **2011**, *5*, 3878–3887.
- [27] R. de la Rica, A. H. Velders, *Small* **2011**, *7*, 66–69.
- [28] T. Premkumar, Y. Lee, K. E. Geckeler, *Chem. Eur. J.* **2010**, *16*, 11563–11566.
- [29] X. Lu, E. Masson, *Langmuir* **2011**, *27*, 3051–3058.
- [30] M. Cao, J. Lin, H. Yang, R. Cao, *Chem. Commun.* **2010**, *46*, 5088–5090.
- [31] S. Helveg, C. Lopez-Cartes, J. Sehested, P. L. Hansen, B. S. Clausen, J. R. Rostrup-Nielsen, F. Abild-Pedersen, J. K. Nørskov, *Nature* **2004**, *427*, 426–429.
- [32] J. A. Rodríguez-Manzo, C. Pham-Huu, F. Banhart, *ACS Nano* **2011**, *5*, 1529–1534.
- [33] Ç. Ö. Girit, J. C. Meyer, R. Erni, M. D. Rossell, C. Kisielowski, L. Yang, C.-H. Park, M. F. Crommie, M. L. Cohen, S. G. Louie, A. Zettl, *Science* **2009**, *323*, 1705–1708.
- [34] P. Mulvaney, M. Giersig, T. Ung, L. M. Liz-Marzán, *Adv. Mater.* **1997**, *9*, 570–575.
- [35] J. Kim, I.-S. Jung, S.-Y. Kim, E. Lee, J.-K. Kang, S. Sakamoto, K. Yamaguchi, K. Kim, *J. Am. Chem. Soc.* **2000**, *122*, 540–541.
- [36] M. Ray, S. Paria, *Ind. Eng. Chem. Res.* **2011**, *50*, 11601–11607.
- [37] D. Jiao, N. Zhao, O. A. Scherman, *Chem. Commun.* **2010**, *46*, 2007–2009.
- [38] G. L. Bottger, C. V. Damsgard, *Solid State Commun.* **1971**, *9*, 1277–1280.
- [39] E. Blanco, C. Quintana, P. Hernández, L. Hernández, *Electroanalysis* **2010**, *22*, 2123–2130.
- [40] J. W. Lee, S. Samal, N. Selvapalam, H.-J. Kim, K. Kim, *Acc. Chem. Res.* **2003**, *36*, 621–630.
- [41] E. González, J. Arbiol, V. F. Puntes, *Science* **2011**, *334*, 1377–1380.
- [42] Y. Ridelman, G. Singh, R. Popovitz-Biro, S. G. Wolf, S. Das, R. Klajn, *Small* **2012**, *8*, 654–660.
- [43] G. Loget, A. Kuhn, *J. Mater. Chem.* **2012**, DOI:10.1039/C2JM31740K.

Received: March 12, 2012  
Revised: May 7, 2012  
Published online: